First-Principles Study of the (001) Surface of Cubic $SrHfO_3$ and $SrTiO_3$

Yuan Xu Wang,*,†,‡ C. L. Wang,‡ and W. L. Zhong‡

Computational Materials Science Center, National Institute for Materials Science, Tsukuba 305-0044, Japan, and School of Physics and Microelectronics, Shandong University, Jinan 250100, People's Republic of China

Received: March 29, 2005; In Final Form: May 9, 2005

We have performed first-principles calculations on the (001) surface of cubic $SrHfO_3$ and $SrTiO_3$ with SrO and BO_2 (B = Ti or Hf) terminations. Surface structure, partial density of states, band structure, and surface energy have been obtained. For the BO_2-terminated surface, the largest relaxation appears on the second-layer atoms but not on the first-layer ones. The analysis of the structure relaxation parameters reveals that the rumpling of the (001) surface for $SrHfO_3$ with SrO termination is stronger than that for $SrTiO_3$. For the HfO_2-terminated surface of $SrHfO_3$, the surface state appears near the *M* point of its band structure.

I. Introduction

Thin ferroelectric films with the ABO_3 perovskite structure used for numerous high-tech applications (such as high-capacity memory cells, optical waveguides, etc.) have been studied theoretically as well as experimentally. In recent years, first-principles studies on the surfaces of ferroelectrics have greatly enhanced the understanding of surface effects on their ferroelectricity and other properties.

Because of their use as the substrate for growing epitaxial films of high critical temperature (T_c) superconductors, the (001) surfaces of $SrTiO_3$ have been extensively studied by various experimental[1−4] and theoretical methods.[5−12] The calculated surface energies[12] and the thermodynamic potential[5] show that both SrO- and TiO_2-terminated surfaces are stable and equally energetically favorable. In SrO- and TiO_2-terminated surfaces, the metal atoms (Sr or Ti) in the first layer relax inward (i.e., toward the bulk), whereas those in the second layer relax outward. For the SrO-terminated surface, it was found from previous calculations that the largest relaxation occurs on the first-layer atoms. The calculated band structures of the (001) surface of cubic $SrTiO_3$ show that the surface states appear on the TiO_2-terminated surface, especially at the *M* point. The covalency of the Ti−O bonds is enhanced near the surface. Padilla and Vanderbilt[5] studied the surface influence on the ferroelectricity of $SrTiO_3$ and found no large ferroelectric distortion in the surface layer of the SrO-terminated surface. For the TiO_2-terminated surface, the ferroelectric instability is so weak that it can be easily destroyed by thermal fluctuations. The ab initio study on the (110) surface of $SrTiO_3$[13] shows that the surface relaxation of the (110) surface is much larger than that of the (100) surface and that there is a considerable increase in the Ti−O bond covalency near the (110) surface relative to bulk $SrTiO_3$, much larger than that for the (100) surface.

$SrHfO_3$ is a compound that has a composition and lattice structure that is very similar to that of $SrTiO_3$. Studying the surface of $SrHfO_3$ and comparing it with $SrTiO_3$ are helpful to understand the surface effect on ferroelectrics. To our knowledge, there is no theoretical study on the (001) surface structure of cubic $SrHfO_3$ by first-principles calculations.

In this paper, we focus on the structure relaxation and the electronic structure of the (001) surface for cubic $SrHfO_3$ (SHO) and $SrTiO_3$ (STO) simulated by the full potential linearized augmented plane wave (FLAPW) method. Regarding the computational method used in our calculations, details are described in section II. The structure, the partial density of states (DOSs), and the band structure are analyzed in section III. The conclusion is given in the last section.

II. Approach

The calculations presented in this work were performed within the local density approximation (LDA)[14] and the generalized gradient approximation (GGA)[15] to the density functional theory, via the FLAPW method. In this method, no shape approximation is made on either the potential or the electronic charge density. The calculations were done with the WIEN2K code,[16] which allows for the inclusion of local orbits in the basis, thus improving upon linearization and making a consistent treatment of semicore and valence states in one energy window possible, hence ensuring proper orthogonality. In the FLAPW method, the unit cell is divided into two parts: (1) nonoverlapping atomic spheres (centered at the atomic sites) and (2) an interstitial region. The FLAPW method expands the potential in the following form:

$$V(r) = \begin{cases} \sum_{lm} V_{lm}(r) Y_{lm}(\hat{r}) & \text{inside sphere} \\ \sum_{K} V_K e^{iKr} & \text{outside sphere} \end{cases} \quad (1)$$

in which $Y_{lm}(\hat{r})$ is a spherical harmonic.

The atomic sphere radii (R_i) of 1.8, 1.8, 1.7, and 1.6 au, were used for Sr, Hf, Ti, and O, respectively, in our calculations. The convergence parameter RK_{max} (R_{mt}·K_{max}, in which K_{max} is the plane wave cutoff and R_{mt} is the smallest of all atomic sphere radii), which controls the size of the basis sets in these calculations, was set to 7.0. This provides well-converged basis sets consisting of approximately 7671 and 6591 plane waves in the surfaces of SHO and STO, respectively. The calculations were iterated to self-consistency with the specified energy

* To whom correspondence should be addressed. Phone: +81-29-851-3354-8092. Fax: +81-29-854-1207. E-mail: wang.yuanxu@nims.go.jp.
† National Institute for Materials Science.
‡ Shandong University.

10.1021/jp0515840 CCC: $30.25
Published on Web 06/09/2005

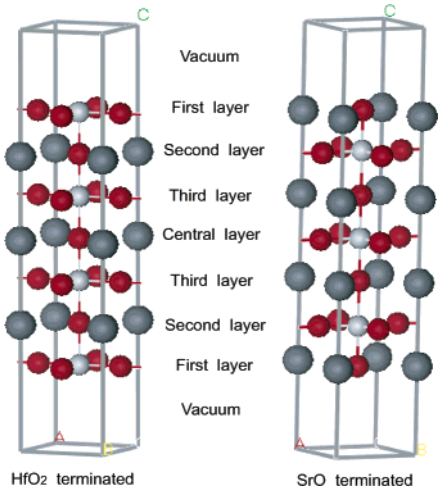

Figure 1. Unit cell for the surface structure of cubic $SrBO_3$ (B = Hf or Ti): the dark gray, red, and light gray colored spheres represent the Sr, O, and B atoms, respectively.

convergence criterion 0.00001 Ry. We used the 12 × 12 × 2 mesh for the Brillouin Zone integration, which represents 21 k-points in its irreducible part.

In our calculations, two types of terminations were considered: SrO termination and BO_2 termination. The periodic boundary condition was used in the calculation with the repeated slab model. For the SrO-terminated surface, the slab consists of four SrO layers and three BO_2 layers, and for the BO_2-terminated one, the slab consists of four BO_2 layers and three SrO layers. For both cases, the slabs with five-lattice-constant thickness are separated by a two-lattice-constant vacuum region and are tetragonal with space group *P*4*mmm*. The unit cell of the (001) surface structure of SHO and STO is displayed in Figure 1. Regarding the charge neutrality of the SrO, HfO_2, and TiO_2 layers, each layer is neutral and so is each slab if the nominal ionic valence is assumed. During the surface structure optimization, all atoms are fully relaxed with the forces less than 2 mRy/au. Enlarging the vacuum region to three times the theoretical lattice constant thickness and increasing the number of layers to 9 only made a difference in the value of *s* (defined below), which was 0.004 Å for the SrO-terminated surface of SHO. This result shows that the vacuum region and the number of layers are large enough for these systems.

Before starting the surface calculations, we optimized the bulk structure by the same method and the same computational conditions with the 10 × 10 × 10 k-point mesh. The computed ground-state structural lattice constants of cubic SHO with GGA and LDA are 4.16 and 4.07 Å, respectively, and are similar to the lattice constant obtained experimentally, 4.12 Å. In the case of cubic STO, the theoretical lattice constant a_0 with LDA is 3.86 Å, which is only 1% smaller than the experimental one (3.89 Å), whereas that with GGA is 3.95 Å. We used the theoretical lattice constants in all calculations presented here.

III. Results and Discussion

A. Structure Relaxation. We first discuss the structural relaxations of the SrO- and TiO_2-terminated surfaces. Table 1 and Table 2 illustrate our calculated atomic relaxations of the SrO-terminated and BO_2-terminated surface structures for the cubic SHO and STO, respectively. As seen from the two tables, for the SrO-terminated surface, the Sr atoms move inward (toward the bulk) and the B (Ti or Hf) atoms move outward (toward the vacuum). The largest relaxation occurs on the surface-layer atoms, as expected. The (001) surface of cubic STO has also been studied by the plane wave pseudopotential (PWP) method.[5,8] For the SrO-terminated surface, the results show that the Sr atoms in the first layer move inward 5.7%[5] and 6.6%.[8] Thus, the results of the SrO-terminated surface for STO by the FLAPW and PWP methods are very similar.

TABLE 1: Calculated Atomic Displacements[a] (δ_z) for the SrO- and HfO_2-Terminated Surfaces of SHO[b]

layer	SrO termination	δ_z LDA	δ_z GGA	HfO_2 termination	δ_z LDA	δ_z GGA
1	Sr	6.7	7.3	Hf	2.8	3.3
	O	−0.7	−0.0029	O	3.0	2.5
2	Hf	−1.5	−1.2	Sr	−3.1	−4.0
	O	−0.2	−0.0058	O	−0.02	−0.003
3	Sr	1.2	1.4	Hf	0.4	0.6
	O	−0.1	0.08	O	0.1	0.2

[a] Relative to the ideal position. [b] Units are in percent of the theoretical lattice constant (a_0 = 4.07 and 4.16 Å for LDA and GGA, respectively). δ_z is positive for the displacement toward the bulk.

TABLE 2: Calculated Atomic Displacements[a] (δ_z) for the SrO- and TiO_2-Terminated Surfaces of STO[b]

layer	SrO termination	δ_z LDA	δ_z GGA	TiO_2 termination	δ_z LDA	δ_z GGA
1	Sr	5.6	6.0	Ti	2.6	3.5
	O	−0.2	0.07	O	0.68	1.2
2	Ti	−1.3	−1.5	Sr	−3.4	−3.8
	O	−0.04	−0.31	O	−0.23	0.1
3	Sr	1.2	1.2	Ti	0.4	0.8
	O	0.06	0.09	O	0.1	0.3

[a] Relative to the ideal position. [b] Units are in percent of the theoretical lattice constant (a_0 = 3.86 and 3.95 Å for LDA and GGA, respectively). δ_z is positive for the displacement toward the bulk.

TABLE 3: Surface Relaxation Parameters[a] for SHO and STO

		s	Δd_{12}	Δd_{23}
	SrO termination			
SHO	this work (LDA)	7.33	−8.11	2.69
SHO	this work (GGA)	7.34	−8.56	2.61
STO	this work (LDA)	5.85	−6.91	2.49
STO	this work (GGA)	5.96	−7.49	2.71
	LDA PWP (ref 5)	5.8	−6.9	2.4
	LDA PWP (ref 8)	7.6	−8.4	2.45
	B3PW (ref 10)	5.66	−6.58	1.75
	BO_2 termination (B = Hf or Ti)			
SHO	this work (LDA)	−0.19	−5.86	3.45
SHO	this work (GGA)	0.79	−7.31	4.62
STO	this work (LDA)	1.89	−5.93	3.77
STO	this work (GGA)	2.37	−7.33	4.54
	LDA PWP (ref 5)	1.8	−5.9	3.2
	LDA PWP (ref 8)	1.78	−6.4	4.7
	B3PW (ref 10)	2.12	−5.79	3.55

[a] In percent of lattice constant a_0.

In the case of BO_2 termination, the largest relaxation occurs on the second-layer atoms but not on the very first-layer ones. For the TiO_2-terminated surface of STO, although our results of the displacement for each atom are slightly different from the previous ones,[5,8] the surface relaxation parameters (*s*, Δd_{12}, and Δd_{23}) are in good agreement.

In Table 3, we present the calculated structural parameters of the two types of surfaces of SHO and STO. For a comparison, the earlier calculations of the cubic STO by LDA-PWP[5,8] and B3PW[10] are also presented. Rumpling parameter *s* measures the outward displacement of the first-layer oxygen with respect to the first-layer metal atoms, and Δd_{12} is the change of the first interlayer spacing, as measured from the surface to the subsurface metal z-coordinate; similar definition is given to Δd_{23} between the second and third layers. Our calculated values of

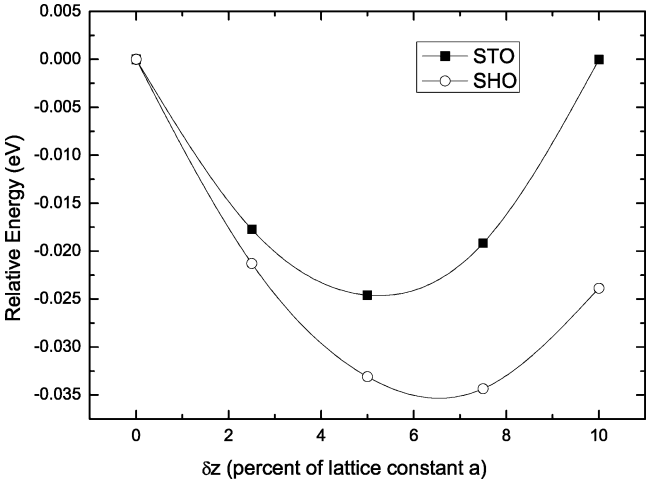

Figure 2. Total energy as a function of the displacement δz (units: relative to the lattice constant a_0) of the Sr atoms in the first layer along the [001] direction for the SrO-terminated surface structures of SHO and STO.

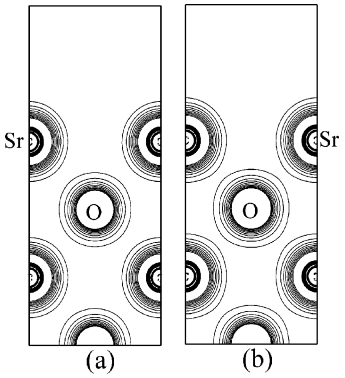

Figure 3. Valence charge density map in the (100) plane of the unrelaxed SrO-terminated surfaces for (a) SHO and (b) STO. The contour interval is 0.2 electrons/Å.

s, Δd_{12}, and Δd_{23} for STO are similar to those of previous reports.[5,8,10] For the SrO-terminated surface, the surface rumpling in SHO is larger than that in STO. In the case of BO_2-termination, our calculated values of s, Δd_{12}, and Δd_{23} show that the rumpling of the BO_2-terminated surface for SHO is smaller than that for STO. The calculated structure parameters for both types of surfaces of SHO and STO by LDA are similar to those calculated by GGA.

We then needed to consider why, for the SrO-terminated surface, the displacement of the Sr atoms for SHO is larger than that for STO during surface rumpling? To understand such behavior, we calculated the total energy of the (001) surface systems for SHO and STO with different displacements of the Sr atoms in the surface layer, and the results are shown in Figure 2. This figure shows that the total energy of the surface structure for SHO decreases more quickly than that of STO with the same displacement of the Sr atoms, which means that the Sr atoms in the SrO-terminated surface of SHO can be more easily moved or that the Sr atoms of the SHO surface with the SrO termination are more flexible. Figure 3 illustrates the valence charge density map in the (100) plane of the unrelaxed SrO-terminated surfaces for SHO (a) and STO (b). As seen in this figure, the region of valence electrons around the Sr atoms in SHO is smaller than that in STO, which implies that the Sr atoms in the surface layer of SHO are more movable than the Sr atoms in the surface layer of STO. For the BO_2-terminated surface, the smaller s of SHO is mainly due to the large displacement of the O atoms in the first layer. The O atoms in the first layer of the HfO_2-terminated surface for SHO move inward ~3% of the theoretical lattice constant, which is much larger than that in STO (0.68% of the lattice constant a_0). The total energy for the (001) surfaces of SHO and STO with BO_2 termination as a function of the displacement of the O atoms along the [001] direction is shown in Figure 4. This figure shows that the total energy of the surface structure for SHO decreases more quickly than that for STO with the same displacement of the O atoms, which means that the O atoms in the first layer of the BO_2-terminated surface for SHO can be moved around more easily.

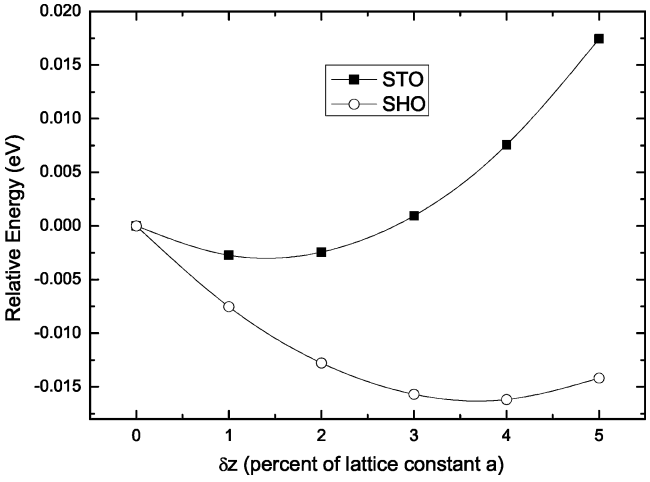

Figure 4. Total energy as a function of displacement δ_z (units: percent of the lattice constant a_0) of the O atoms in the first layer along the [001] direction for the BO_2-terminated surface structures of SHO and STO.

B. Surface Electronic Structure. Figure 5 displays the surface band structures for the SrO- and HfO_2-terminated relaxed surface structures with the band structure of cubic SHO. For the two types of surfaces structures, the calculated energy bands are uniformly shifted so that the 1s core level energy of the metal atom in the central layer is aligned with that in the bulk system. The calculated band gaps for the SrO- and HfO_2-terminated surfaces of SHO are 3.25 and 3.2 eV, respectively. The indirect band gaps for the surfaces and the bulk of the two materials are listed in Table 4. Thus, the band gaps for the SrO- and HfO_2-terminated surfaces are reduced in comparison with that in the bulk system. Compared with the bulk system, there is a tendency in the BO_2-terminated surface for the band states of O p around 0 eV to extend upward, especially at the M point. From this point of view, it can be deduced that the surface state appears at the M point.

To further understand the behavior of the band structures for the two types of surface structures, we have calculated the partial DOSs, and the results are shown in Figures 6 and 7. As can be seen in Figure 6, compared with the DOS of the O atoms in the central layer, the peak of O p in the surface layer obviously shifts to higher energy, which indicates that the reduction of the band gap of the BO_2-terminated surface is mainly due to the upward shift of the O p bands in the surface layer. For the BO_2-terminated surface, the behavior of the surface states is almost the same as that of STO reported by Padilla[5] and Heifets et al.[11]

C. Surface Energies. We define E_s as the average surface energy of two types of surface termination:

$$E_s = \frac{1}{4}[E_{slab}(I) + E_{slab}(II) - 7E_{bulk}], \qquad (2)$$

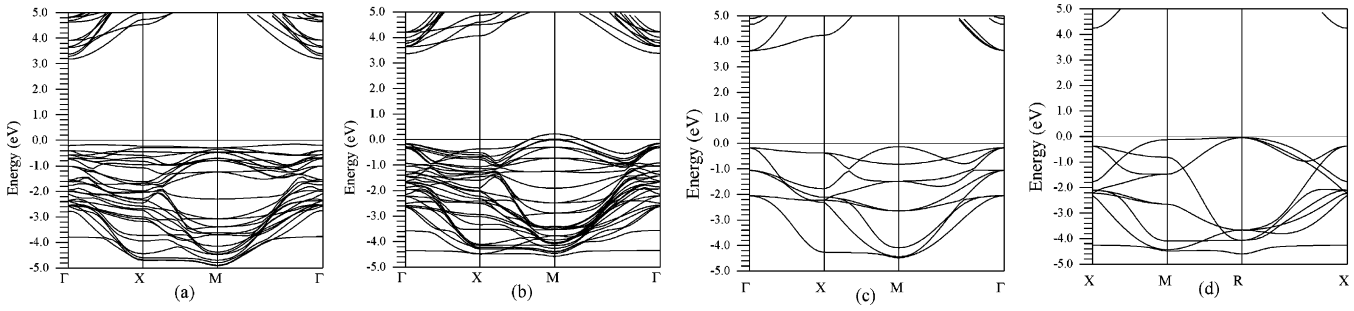

Figure 5. Band structure for SHO: (a) SrO-terminated surface. (b) HfO_2-terminated surface. (c) Bulk band structure of $\Gamma \rightarrow X \rightarrow M \rightarrow \Gamma$. (d) Bulk band structure of $X \rightarrow M \rightarrow R \rightarrow X$. The top of the valence bands for the bulk system is set at zero.

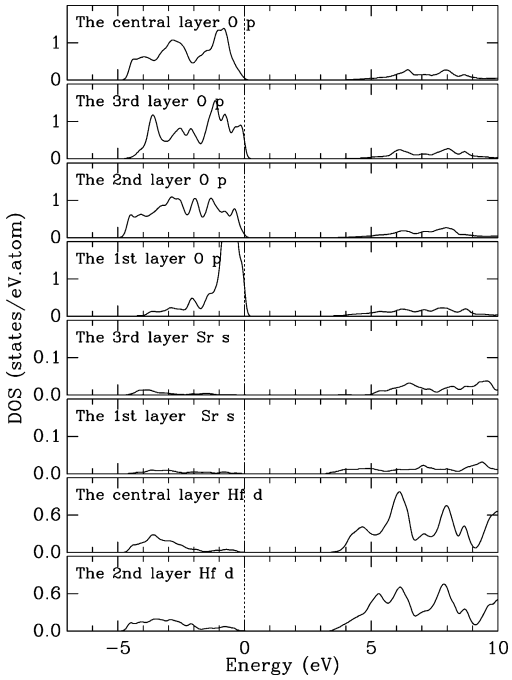

Figure 6. Partial DOSs for each layer of the SrO-terminated surface of SHO.

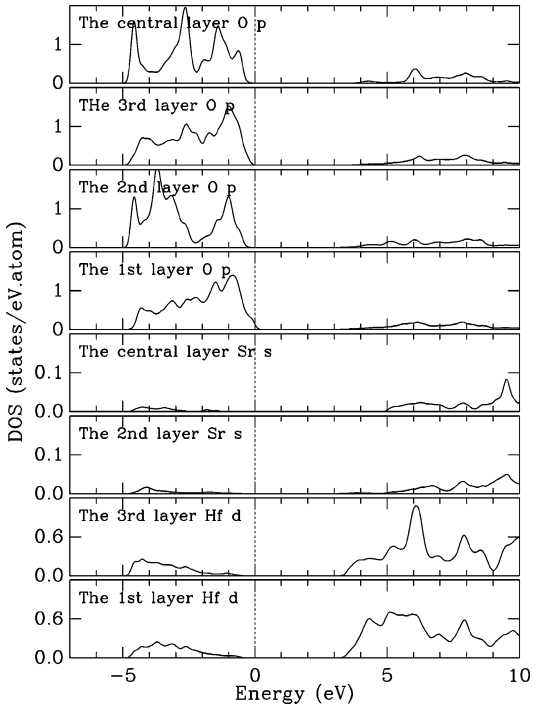

Figure 7. Partial DOSs for each layer of the HfO_2-terminated surface of SHO.

TABLE 4: Calculated Band Gaps (in eV) for the SrO-Terminated Surfaces, the BO_2-Terminated Surfaces, and Bulk of SHO and STO

	SrO termination	BO_2 termination	bulk
SHO-GGA	3.15	3.2	3.7
SHO-LDA	3.25	3.2	3.6
STO-GGA	1.8	1.1	1.8
STO-LDA	1.8	1.2	1.8

in which $E_{slab}(I)$, $E_{slab}(II)$, and E_{bulk} are the total energies of the relaxed SrO-terminated slab, the relaxed BO_2-terminated slab, and the bulk crystal per unit cell, respectively. A factor of 4 is derived from the fact that we create four surfaces during the cleavage procedure. The number 7 in our calculations means that the two seven-layered SrO- and BO_2-terminated surfaces together represent seven bulk unit cells. The average surface energy, the cleavage energy, and the relaxation energy of SHO and STO are listed in Table 5 together with those obtained by LDA-PWP for STO[5,8] for a comparison. The cleavage energy (E_{cle}) and the relaxation energy (E_{rel}) are defined as

$$E_{cle} = \frac{1}{4}[E_{slab}^{(unrel)}(I) + E_{slab}^{(unrel)}(II) - 7E_{bulk}] \quad (3)$$

$$E_{rel}(I) = \frac{1}{2}[E_{slab}(I) - E_{slab}^{(unrel)}(I)] \quad (4)$$

TABLE 5: Theoretical Average Surface Energies for SHO and STO (in eV/a_0^2)[a]

	E_{cle}	E_{rel} (I)	E_{rel} (II)	E_s
SHO-GGA	1.36	−0.24	−0.19	1.15
SHO-LDA	1.62	−0.28	−0.17	1.40
STO-GGA	1.18	−0.19	−0.18	1.00
STO-LDA	1.45	−0.20	−0.15	1.28
STO-LDA-PWP (ref 5)				1.26
STO-LDA-PWP (ref 8)		−0.3	−0.14	1.21

[a] E_{cle} means the cleavage energy, and E_{rel} is the relaxation energy.

in which $E_{slab}^{(unrel)}(I)$, $E_{slab}^{(unrel)}(II)$, and $E_{slab}(I)$ are the total energies for the unrelaxed SrO-terminated slab, the unrelaxed BO_2-terminated slab, and the relaxed SrO-terminated slab, respectively. From Table 5, we can easily see that the cleavage energies of SHO are larger than that of STO. The relaxation energies of the BO_2-terminated surface for the two materials are similar, whereas those of the SrO-terminated surface are different. The absolute values of the relaxation energies of SHO are larger than those of STO. The surface energy of SHO is larger than that of STO. The smaller surface energy means easier cleavability under the condition that the migration of atoms can be neglected. Thus, the surface of STO is easier to construct. Our calculated value of E_s for STO by LDA agrees well with the previous calculations by the LDA-PWP method.[5,8]

IV. Conclusion

From the structure and electronic structure properties of the SrO- and BO_2-terminated (001) surfaces of SHO and STO obtained from the FLAPW method within LDA and GGA, we found that for the BO_2-terminated surface, the largest relaxation is observed on the second-layer atoms and not on the first-layer ones. The analysis of the structure relaxation parameters reveals that the rumpling of the SrO-terminated surface structure for SHO is stronger than that for STO. The surface rumpling of the BO_2-terminated surface for SHO is much smaller than that for STO, which is mainly due to the large displacement of the O atoms in the surface layer of SHO. Comparing the band structures of the HfO_2-terminated surface of SHO with that of the bulk system reveals that the surface state appears near the *M* point of its band structure. Compared to SHO, the smaller surface energy in STO indicates that the surface of STO is more easily constructed. These findings could be important for the structure of surface defects as well as for the adsorption and surface diffusion of atoms and small molecules relevant for catalysis.

Acknowledgment. The calculations were performed on the Numerical Materials simulator at National Institute for Materials Science. This work is supported by the National Natural Science Foundation of China under Project No. 10474057.

References and Notes

(1) Bickel, N.; Schmidt, G.; Heinz, K.; Müller, K. *Phys. Rev. Lett.* **1989**, *62*, 2009−2011.
(2) Hikita, T.; Hanada, T.; Kudo, M.; Kawai, M. *Surf. Sci.* **1993**, *287*−*288*, 377−381.
(3) van der Heide, P. A. W.; Jiang, Q. D.; Kim, Y. S.; Rabalais, J. W. *Surf. Sci.* **2001**, *473*, 59−70.
(4) Maus-Friedrichs, W.; Frerichs, M.; Gunhold, A.; Krischok, S.; Kempter, V.; Bihlmayer, G. *Surf. Sci.* **2002**, *515*, 499−506.
(5) Padilla, J.; Vanderbilt, D. *Surf. Sci.* **1998**, *419*, 64−70.
(6) Ravikumar, V.; Wolf, D.; Dravid V. P. *Phys. Rev. Lett.* **1995**, *94*, 960−963.
(7) Li, Z. Q.; Zhu, J. L.; Wu, C. Q.; Tang, Z.; Kawazoe, Y. *Phys. Rev. B* **1998**, *58*, 8075−8078.
(8) Cheng, C.; Kunc, K.; Lee, M. H. *Phys. Rev. B* **2000**, *62*, 10409−10418.
(9) Heifets, E.; Eglitis, R. I.; Kotomin, E. A.; Maier, J.; Borstel, G. *Phys. Rev. B* **2001**, *64*, 235417.
(10) Eglitis, R. I.; Piskunov, S.; Heifets, E.; Kotomin, E. A.; Borstel, G. *Ceram. Int.* **2004**, *30*, 1989−1992.
(11) Heifets, E.; Eglitis, R. I.; Kotomin, E. A.; Maier, J.; Borstel, G. *Surf. Sci.* **2002**, *513*, 211−220.
(12) Piskunov, S.; Kotomin, E. A.; Heifets, E.; Maier, J.; Eglitis, R. I.; Borstel, G. *Surf. Sci.* **2005**, *575*, 75−88.
(13) Heifets, E.; Goddard, W. A., III; Kotomin, E. A.; Eglitis, R. I.; Borstel, G. *Phys. Rev. B* **2004**, *69*, 035408.
(14) Desclaux, J. P. *Comput. Phys. Commun.* **1975**, *9*, 31−45.
(15) Perdew, J. P.; Burke, S.; Ernzerhof, M. *Phys. Rev. Lett.* **1996**, *77*, 3865−3868.
(16) Blaha, P.; Schwarz, K.; Luitz, J. *WIEN2K*; *An Augmented Plane Wave + Local Orbitals Program for Calculating Crystal Properties*; Vienna University of Technology: Vienna, Austria, 2001.